A multiscale medium approximation method for the propagation P-waves in highly heterogeneous geophysical media

Théophile Chaumont-Frelet, Hélène Barucq, Henri Calandra, Christian Gout

A MULTISCALE MEDIUM APPROXIMATION METHOD FOR THE PROPAGATION P-WAVES IN HIGHLY HETEROGENEOUS GEOPHYSICAL MEDIA

T. CHAUMONT-FRELET[1,2,3], H. BARUCQ[1,4], H. CALANDRA[5], AND C. GOUT[2]
[1] MAGIQUE3D, INRIA RESEARCH CENTRE BORDEAUX SUD-OUEST
[2] NORMANDIE UNIVERSITE, INSA ROUEN NORMANDIE, LMI
[3] BASQUE CENTER FOR APPLIED MATHEMATICS,
[4] UNIVERSITY OF PAU
[5] TOTAL E&P

Abstract. Approximating the solution of Helmholtz problems is a tricky task, especially at high frequency. Indeed, because of the numerical dispersion, it is mandatory to increase the number of discretization points per wavelength for higher frequencies. Using high degree polynomial shape functions on a coarse mesh is an interesting approach because it contributes to reduce such numerical dispersion as compared to linear functions set on a fine mesh. While this solution is very efficient for wave propagation in homogeneous media, it is not obvious how the variations of the medium inside a cell have to be taken into account. Recently the Multiscale Medium Approximation method (MMAm) has been proposed to overcome this difficulty. High-order shape functions are used with a coarse mesh to reduce dispersion and hence, the pollution effect. Then, the key idea is to introduce a multiscale approximation of the medium to take into account fine scale heterogeneities on the coarse mesh. This approach has proven to be efficient on academic test cases and a convergence theory has been developed. In this work, we further validate the MMAm by demonstrating its efficiency on geophysical benchmarks. Highly heterogeneous media, Seismic wave propagation, Time-harmonic modelling, High-order methods, Mulsticale methods, Finite element methods

1. Introduction

Wave propagation is a physical phenomenon that has demonstrated very good skills for imaging structures that we cannot see with our own eyes. It is now used in a wide variety of applications which aim at recovering the physical characteristics of the propagation medium. For instance, seismic imaging is a powerful tool for prospection of resources. An image of the Earth subsurface can be obtained based on surface observations only. The procedure involves seismic waves, which bring information back to the surface because reflections occur when the wave front encounters an interface in the ground. The analysis of the huge amount of data generated in seismic campaigns is a tricky task which requires in particular optimized wave equation solvers. Into the Earth, wave propagation is indeed a complex phenomenon which is difficult to reproduce numerically. Any simulation has to be accurate to avoid representing artifacts and in the same time, it has to be fast to provide a tool usable in real time.

In this work, we will focus on time-harmonic wave propagation, having in mind Full Waveform Inversion as an application. Different numerical schemes are possible to approximate the harmonic wave operator. Finite difference approximations are the most widely used by oil industry because they are easy to implement as compared to finite element approximations [19]. However, geophysical media can include topography effects which impact on the wave propagation and finite difference grids have difficulties to take topography into account.

Having in mind to simulate the propatation of P-waves in heterogeneous media including topography, it seems relevant to use finite element approximations. But then, two major difficulties occur. First, because of numerical dispersion, accurate modeling of high frequency waves is computationally expensive. Second, taking into account fine scale variations of the propagation medium

can be a challenging issue. These two problems have motivated the development of robust solvers for the Helmholtz equation [3].

Numerical dispersion has been the subject of intense research and is now well understood in homogeneous media. As shown in [1], if the mesh is not sufficiently refined, numerical waves propagate at a wrong speed. As a result the number of points per wavelength must be increased for high frequencies to accurately capture oscillations with a correct wavespeed. Though advanced methods have been introduced to reduce the pollution effect drastically, they are usually designed for cartesian grids in homogeneous media (see for instance [5]). Unfortunately, their application to unstructured meshes and heterogeneous media is not trivial. Nevertheless, it has been observed that classical high order polynomial discretizations can reduce the pollution effect significantly compared to linear elements (see [17, 20] for instance).

High order methods are also used in Geophysics to model accurately high frequency waves. However, a problem arise in highly heterogeneous media. Indeed, high order methods are used with coarse meshes, and it might be challenging to take into account fine scale heterogeneities.

Periodic homogenization techniques have been applied to upscale fine scale properties of the Earth. They permit to get an "effective" propagation medium that can be meshed easily. Under restrictive assumptions of periodicity, the homogenization process is well understood and convergence analysis is available (see [2,16] for instance). In Geophysics, the idea dates back to [6] where the author showed that fine scale isotropic layers can be upscaled into a homogeneous anisotropic medium. Periodic homogenization has two main drawbacks. First, the medium parameter are supposed to be periodic. Though it is possible to weaken the assumption of periodicity, a special structure of the medium, which is usually unrealistic for geophysical applications, is always required in homogenization. Second, a separation of scales between the wavelength and the spatial period of the heterogeneities is required. This last point has been quantitatively analysed in [13]. They showed that the anisotropic approximation of Backus is valid only if the wavelength is at least five times larger than the spatial period of the heterogeneities.

The periodicity hypothesis can actually be dropped. In recent developments, Capdeville and collaborators have introduced a non-periodic homogenization framework in a series of papers [9–12]. The procedure is based on a user defined parameter λ_0 which separates the microscopic and macroscopic scales. The homogenization procedure includes a low-pass filtering to upscale properties of the medium under the wavelength λ_0.

The aim of the present paper is to investigate an alternative to homogenization previously introduced in [8], the so-called Multiscale Medium Approximation method (MMAm) and to figure out how the MMAm performs on geophysical examples. According to [8], the MMAm makes it possible to include the variations of the medium when using a coarse grid. By this way, high-degree polynomial shape functions can be used and the MMAm thus withstands pollution effects. The key idea is to apply a well-suited quadrature formula on a fine but fictive grid which does not generate increased computational costs to take into account fine scale heterogeneities. The convergence analysis of the MMAm is available in [14, 15]. In particular, the method is shown to be robust with respect to numerical dispersion, even in highly heterogeneous media.

The key feature of the proposed method is its simplicity. As a result, the method is easily implemented in a parallel fashion, and turns out to be computationally efficient. Actually, the resulting algorithms are nearly as simple to implement as a standard FEm, and can be easily included in an existing finite element code. Here, we show that despite its simplicity in design and use, the method is able to efficiently approximate high frequency waves in complex media.

Though we restrict our investigation to time-harmonic acoustic problems, the method has been applied with minor modifications to elastic problems [14]. Furthermore, the method could also be used for time-domain wave propagation problems, if coupled with a discontinuous Galerkin scheme [7].

The paper is organized as follows. In Section 1, we briefly introduce the MMAm. We focus on its implementation, and give all important formulas in a way that it can be implemented efficiently. We also discuss the corresponding computational costs. Sections 2 and 3 are dedicated to geophysical test-cases. Section 2 deals with 2D benchmarks while Section 3 is devoted to a 3D model. In all the cases, we deliver a performance assessment by analyzing both the size and filling

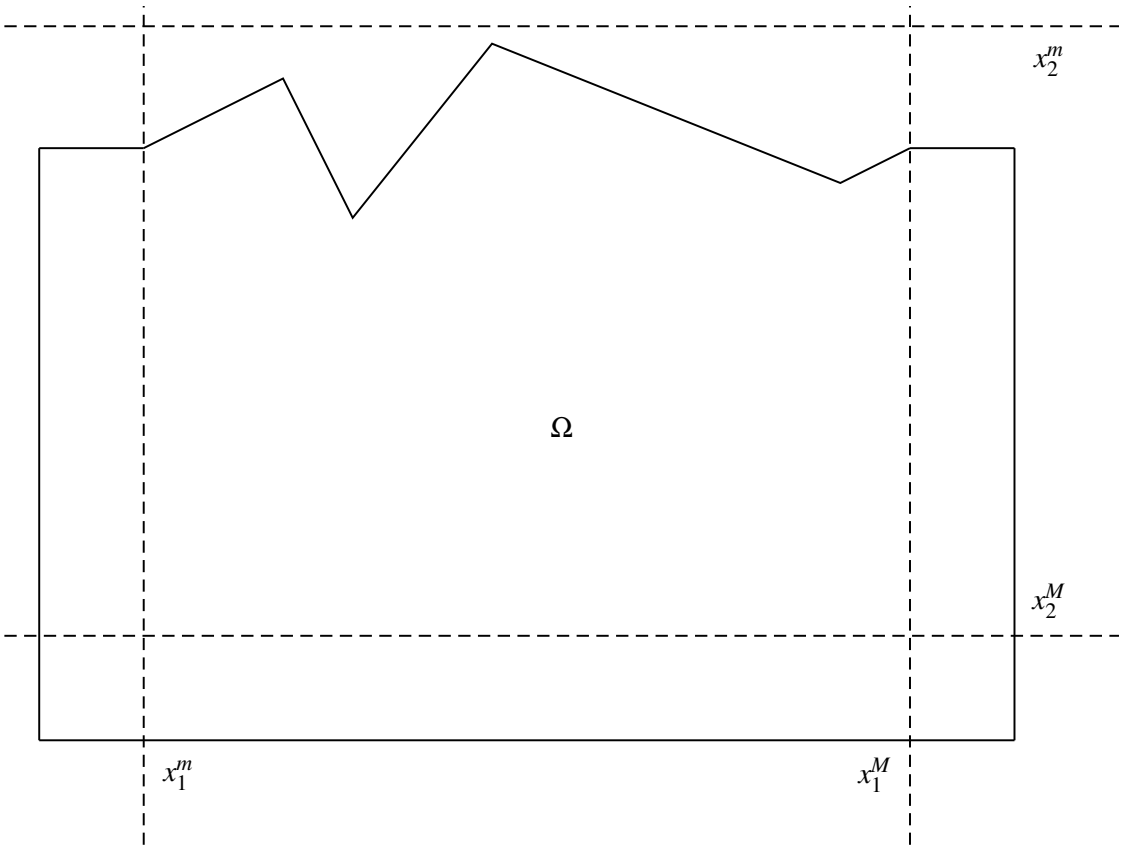

FIGURE 1. Computational domain

of the corresponding linear systems. For the 3D model, computational times are compared as well. The conclusion is that, regarding the benchmarks we have considered, the MMAm significantly outperforms the standard FEm.

2. Presentation of the Multiscale Medium Approximation method

2.1. **Problem setting.** We consider an acoustic Helmholtz equation with constant density. The medium of propagation $\Omega \subset \mathbb{R}^N$ is characterized by the wavespeed $c : \Omega \to \mathbb{R}_+^\star$. A free surface boundary condition is imposed on the top of the domain which represents the surface of the Earth. The rest of the boundary is surrounded by Perfectly Matched Layers (PMLs) of size $L > 0$ to simulate a semi-infinite propagation medium [18]. A sketch of the computational domain is presented on Figure 1.

Hence, given a seismic source g and considering a frequency f, the pressure u is solution to

$$\left\{ \begin{array}{rcll} -\dfrac{d\omega^2}{c^2}u - \operatorname{div}(D\nabla u) & = & g & \text{in } \Omega, \\ u & = & 0 & \text{on } \partial\Omega, \end{array} \right. \tag{1}$$

where $\omega = 2\pi f$ and the coefficients d and D represent the PMLs. These coefficients are defined by

$$d = \prod_{i=1}^{N} \xi_i^{-1}, \quad D = d\big(\xi_i \xi_j\big)_{i,j=1}^{N},$$

where

$$\xi_i(x) = \left\{ \begin{array}{ll} 1 & \text{if } x_i^m \leq x_i \leq x_i^M, \\ \dfrac{\mathbf{i}\omega}{\mathbf{i}\omega + \sigma} & \text{otherwise,} \end{array} \right.$$

and $\sigma \in \mathbb{R}_+^*$ is a constant user-defined parameter.

Having in mind geophysical applications where the seismic source is typically local, the considered right-hand-sides g are either Dirac masses, or Gaussian distributions. However, the presented method is not limited to these particular types of right-hand-sides.

Full waveform inversion is one of the main potential applications for the MMAm. Since frequencies ranging from 1 to 10 Hz are typically used for in this inversion process (see, for instance [21]), we consider in this paper frequencies $f \leq 10$ Hz.

2.2. **Abstract finite element formulation.** In this paper, we focus on a finite element discretization of problem (1). Therefore, we classically recast the boundary value problem of interest into a variational problem as follows: find $u \in H_0^1(\Omega)$ such that

$$b(u, v) = \langle g, v \rangle, \quad \forall v \in H_0^1(\Omega), \tag{2}$$

where

$$b(u, v) = -\omega^2 \int_\Omega \frac{d}{c^2} u \overline{v} + \int_\Omega D \nabla u \cdot \overline{\nabla v}. \tag{3}$$

In the following, we focus on a conforming finite element method which relies on a discretization subspace $V_h \subset H_0^1(\Omega)$. We obtain the finite element formulation by replacing $H_0^1(\Omega)$ by the discretization subspace V_h in (2). Hence, the discrete solution $u_h \in V_h$ is sought in the discretization space as the unique element satisfying

$$b(u_h, v_h) = \langle g, v_h \rangle, \quad \forall v_h \in V_h. \tag{4}$$

If $n = \dim V_h$, let $\{\phi_k\}_{k=1}^n$ be a basis of V_h. Problem (4) is equivalent to a $n \times n$ linear system $MU = F$, where $U = \{u_k\}_{k=1}^n$ represents the coefficients of u_h in the basis, that is:

$$u_h = \sum_{k=1}^n u_k \phi_k.$$

The coefficients of M and F are defined by

$$M_{kl} = b(\phi_l, \phi_k), \quad F_k = \langle g, \phi_k \rangle. \tag{5}$$

Thus, the finite element procedure consists in computing the entries of M and F and then solve the linear system. In this regard, it is clear that an efficient finite element method should minimize the size and the filling of M, while ensuring that the entries of M and F are cheap to compute.

2.3. **Standard Lagrangian elements.** Lagrangian finite elements are based on two main ingredients: a reference cell $\hat{K}$ and a reference space $\hat{P}$. In the following, $\hat{K}$ is a triangle in 2D and a tetrahedron in 3D. Furthermore, given $p \in \mathbb{N}^\star$, we consider the reference space $\hat{P} = \mathcal{P}_p(\hat{K})$ of polynomials of degree less or equal than p on $\hat{K}$. We note $\hat{n} = \dim \hat{P}$ and $\{\hat{\psi}_i\}_{i=1}^{\hat{n}}$ the Lagrangian basis of $\hat{P}$.

In order to construct the discretization space V_h, a conforming mesh $\mathcal{T}_h$ of Ω is required. We assume that each cell $K \in \mathcal{T}_h$ is a triangle in 2D or a tetrahedra in 3D. It follows that for each cell $K \in \mathcal{T}_h$, there exists an affine mapping $\mathcal{F}_K : \mathbb{R}^N \to \mathbb{R}^N$ such that $\mathcal{F}_K(\hat{K}) = K$. For every cell $K \in \mathcal{T}_h$, we will note $A_K \in \mathcal{L}(\mathbb{R}^N)$ and $y_K \in \mathbb{R}^N$ the matrix and the vector such that

$$\mathcal{F}_K(x) = A_K x + y_K, \quad \forall x \in \mathbb{R}^2.$$

It is worth noting that since $\mathcal{F}_K$ is affine, the Jacobian $J_{\mathcal{F}_K} = A_K$ is constant.

The discretization space V_h is constructed in three steps:

(a) On each $K \in \mathcal{T}_h$, we consider local basis functions that are the images of functions of $\hat{P}$ through the mapping $\mathcal{F}_K$.
(b) A C^0 compatibility condition is imposed globally to ensure that $V_h \subset H^1(\Omega)$.
(c) The functions that do not vanish on $\partial\Omega$ are removed to ensure that $V_h \subset H_0^1(\Omega)$.

Hence, we have the following definition for V_h:

$$V_h = \left\{ v_h \in C^0(\overline{\Omega}) \;\middle|\; \begin{array}{l} \forall K \in \mathcal{T}_h \\ v_h|_K \circ \mathcal{F}_K^{-1} \in \hat{P} \\ v_h|_{\partial\Omega} = 0 \end{array} \right\}.$$

We note $n = \dim V_h$ and consider the Lagrangian basis $\{\phi_k\}_{k=1}^n$ of V_h. One of the key aspects of Lagrangian finite elements, is that, for each cell K, the restriction of a global basis $\phi_k|_K$ to K, is the image of a local basis function $\hat{\psi}_i$. We can express this by the fact that, for all $K \in \mathcal{T}_h$, there exists an application, called the "global to local numbering" $\mathcal{L}_K : \{1, \dots, n\} \to \{-1\} \cap \{1, \dots, \hat{n}\}$ so that

$$\phi_k|_K = \hat{\psi}_{\mathcal{L}_K(i)} \circ \mathcal{F}_K, \quad \forall k \in \{1, \dots, n\},$$

where we use the simplifying notation $\hat{\psi}_{-1} = 0$.

In order to assemble the finite element linear system M, we need to compute $b(\phi_k, \phi_l)$ for all $k, l \in \{1, \dots, n\}$. In order to simplify this operation, it is assumed that c is constant on each cell $K \in \mathcal{T}_h$ and takes the value c_K. Hence, for $k, l \in \{1, \dots, n\}$, we have

$$M_{kl} = -\omega^2 \sum_{K \in \mathcal{T}_h} \frac{d_K}{c_K^2} \int_K \phi_l \phi_k + \sum_{K \in \mathcal{T}_h} \sum_{i,j=1}^{N} D_K^{ij} \int_K \frac{\partial \phi_l}{\partial x_i} \frac{\partial \phi_k}{\partial x_j}.$$

It is clear that it is possible to compute the coefficients of M analytically from (2.3). Indeed, the integrals in (2.3) involve polynomial functions and can be computed exactly.

As above-mentioned, fast computations of (2.3) is crucial for efficient finite element code. As a matter of fact, the finite element framework comes with an efficient computation methodology that we briefly describe hereafter. In order to lighten the presentation, we will only focus on the first integral of (2.3):

$$\frac{1}{c_K^2} \int_K \phi_k \phi_l, \tag{6}$$

for all $l, k \in \{1, \dots, n\}$ and $K \in \mathcal{T}_h$. The other terms can be treated in the same way.

It is worth noting that since only polynomials are involved, it is possible to directly apply a quadrature formula in each cell to exactly compute (6). Though this methodology is straightforward, it is not efficient because the basis functions need to be explicitly computed and evaluated at the quadrature nodes in each cell. In order to greatly reduce the computational cost, the integrals of the reference basis functions are usually introduced

$$\hat{M}_{ij} = \int_{\hat{K}} \hat{\psi}_i \hat{\psi}_j, \quad \forall i, j \in \{1, \dots, \hat{n}\}. \tag{7}$$

Of course, these coefficients are analytically available. Furthermore, they are only required for the reference cell $\hat{K}$, which means that they can be directly hard-coded in a program. It is also possible to compute the coefficient numerically on the fly at the start of the program execution and since the computations need to be done for the reference cell $\hat{K}$ only, the computational time is not significant.

With the values (7) readily available, it is possible to compute (6) fast with:

$$\int_K \phi_k \phi_l = \frac{|\det A_K|}{c_K^2} M_{\mathcal{L}_K(k)\mathcal{L}_K(l)}, \tag{8}$$

for all $k, l \in \{1, \dots, n\}$ and $K \in \mathcal{T}_h$.

Though the finite element method introduced just before permits to compute the entries of M efficiently thanks to (8), the main drawback is that it is mandatory to assume that the velocity parameter c is constant over each cell $K \in \mathcal{T}_h$. In highly heterogeneous media this is a problem since the mesh has to fit correctly the small-scale variations of the velocity. Then, the mesh size h needs to be chosen to fit all physical interfaces contained in c. This means that in some cases, very small mesh sizes need to be employed, resulting in a very large linear system to solve.

2.4. **The Multiscale Medium Approximation method.** We propose to improve the standard finite element method using a multiscale strategy that we call the MMAm: Multiscale Medium Approximation method [8, 14, 15]. We introduce a second-level approximation for the velocity parameter, characterized by a small parameter ϵ. Our aim is to use the usual finite element space V_h on a coarse mesh. In the MMAm, the choice of h is constrained by the frequency f, but not by the velocity parameter, in the sense that c is allowed to vary inside the cells. The fine-scale variations of c are taken into account thanks to a subcell strategy, characterized by a small parameter ϵ which can be set independently of h. Of course, the interesting case is then $\epsilon \ll h$.

We first need to introduce a submesh of the reference cell $\hat{K}$, denoted by $\hat{\mathcal{T}}_{\hat{\epsilon}}$. We assume that $\hat{\mathcal{T}}_{\hat{\epsilon}}$ is made of $\hat{m}$ triangles or tetrahedron. For the sake of simplicity, we further assume that the elements of the reference submesh are numbered: $\hat{\mathcal{T}}_{\hat{\epsilon}} = \{\hat{C}_s\}_{s=1}^{\hat{m}}$.

The submesh $\hat{\mathcal{T}}_{\hat{\epsilon}}$ is a mesh of the reference cell $\hat{K}$ which will be mapped afterward on each cell K. For this reason, we denote by $\hat{\epsilon}$ the size of the cells of $\hat{\mathcal{T}}_{\hat{\epsilon}}$. The fine-scale is then defined by $\epsilon = h\hat{\epsilon}$.

As we already mentioned, we will use the standard finite element space V_h. In particular, the basis functions $\{\phi_k\}_{k=1}^n$ remain the same. We thus emphasize that the submesh $\hat{\mathcal{T}}_{\hat{\epsilon}}$ is introduced only to better take into account the velocity parameter c.

For each cell $K \in \mathcal{T}_h$, we denote by $\mathcal{T}_\epsilon^K$ the mesh of K obtained by mapping $\hat{\mathcal{T}}_{\hat{\epsilon}}$:

$$\mathcal{T}_\epsilon^K = \left\{ C_s^K = \mathcal{F}_K(\hat{C}_s) \right\}_{s=1}^{\hat{m}}.$$

In the derivation of the standard finite element method, we assume that the velocity c is constant over each $K \in \mathcal{T}_h$. The MMAm is established under the weaker assumption that c is constant over each subcell $C_s^K \in \mathcal{T}_\epsilon^K$, for all $K \in \mathcal{T}_h$. Hence, we assume that

$$c|_{C_s^K} = c_{K,s} \in \mathbb{R}_+^*, \tag{9}$$

for all $K \in \mathcal{T}_h$ and $C_s^K \in \mathcal{T}_\epsilon^K$, or equivalently that

$$c = \sum_{K \in \mathcal{T}_h} \sum_{C_s^K \in \mathcal{T}_\epsilon^K} c_{K,s} \mathbf{1}_{C_s^K},$$

where $\mathbf{1}_{C_s^K}$ is the set function of C_s^K defined as

$$\mathbf{1}_{C_s^K}(x) = \begin{cases} 1 \text{ if } x \in C_s^K, \\ 0 \text{ otherwise.} \end{cases}$$

We point out that the subcells C_s^K are proper subsets of the finite element mesh cells $K \in \mathcal{T}_h$. As a result, the velocity parameter c is allowed to vary inside the mesh cells. In contrast, the standard finite element method relies on the assumption that

$$c = \sum_{K \in \mathcal{T}_h} c_K \mathbf{1}_K,$$

and the wavespeed takes some constant value $c_K \in \mathbf{R}_+^*$ inside each mesh cell $K \in \mathcal{T}_h$.

Under assumption (9), it is still possible to compute the coefficients of the matrix efficiently. Indeed, we have

$$M_{kl} = -\omega^2 \sum_{K \in \mathcal{T}_h} d_K \sum_{s=1}^{\hat{m}} \frac{1}{c_{K,s}^2} \int_{C_s^K} \phi_l \phi_k + \sum_{K \in \mathcal{T}_h} \sum_{i,j=1}^{N} D_K^{ij} \int_K \frac{\partial \phi_l}{\partial x_i} \frac{\partial \phi_k}{\partial x_j},$$

for all $k, l \in \{1, \dots, n\}$, where the standard finite element integral (6) is replaced by

$$\sum_{s=1}^{\hat{m}} \frac{1}{c_{K,s}^2} \int_{C_s^K} \phi_l \phi_k, \tag{10}$$

for all $k, l \in \{1, \dots, n\}$ and $K \in \mathcal{T}_h$.

As in the case of (6), we can compute (10) exactly by applying a quadrature formula on all cells $C_s^K \in \mathcal{T}_\epsilon^K$ and $K \in \mathcal{T}_h$. However, we can make the same remark than in the standard finite element case: this method requires to evaluate the basis functions at every point of a quadrature scheme

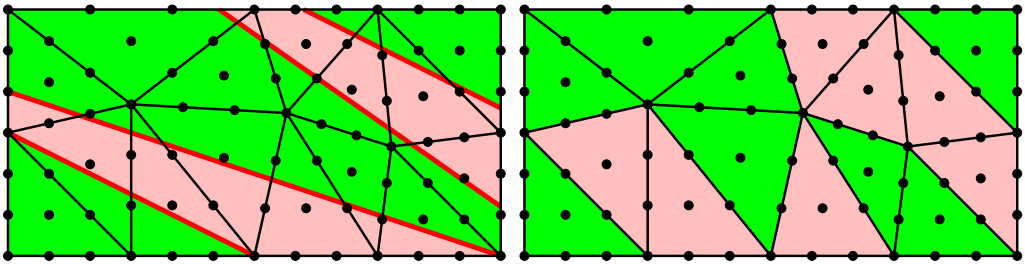

FIGURE 2. The original parameter c (left) and the FEm approximation c_h (right)

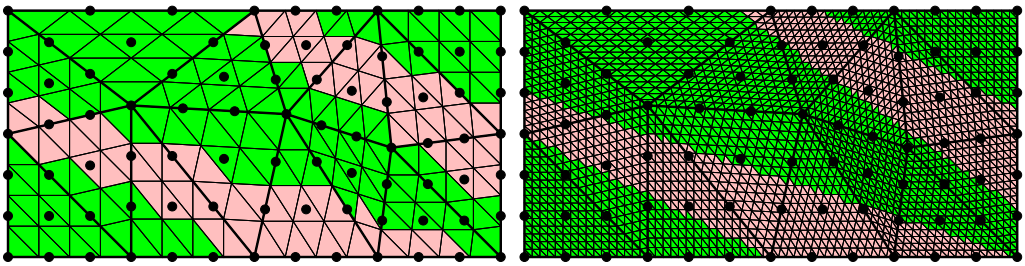

FIGURE 3. MMAm approximation c_ϵ for $\hat{\epsilon} = 1/4$ (left) and $\hat{\epsilon} = 1/16$ (right)

in all mesh cells, which is not efficient. Fortunately, it is possible to improve the computational methodology by introducing the reference integrals:

$$\hat{M}^s_{ij} = \int_{\hat{C}_s} \hat{\psi}_i \hat{\psi}_j, \tag{11}$$

for all $i, j \in \{1, \dots, \hat{n}\}$ and $s \in \{1, \dots, \hat{m}\}$.

The situation is similar to the standard finite element case: the reference values (11) need to be computed on the reference mesh $\hat{\mathcal{T}}_{\hat{\epsilon}}$ only. Therefore, the computational cost for these values is not significant and we can assume that they are readily available. We then have the following efficient formula:

$$\sum_{s=1}^{\hat{m}} \frac{1}{c^2_{K,s}} \int_{C^K_s} \phi_l \phi_k = |\det A_K| \sum_{s=1}^{\hat{m}} \frac{1}{c^2_{K,s}} \hat{M}^s_{\mathcal{L}_K(l)\mathcal{L}_K(k)},$$

for all $k, l \in \{1, \dots, n\}$ and $K \in \mathcal{T}_h$.

In comparison with the standard finite element formula (8), the multiplication by c_K^{-2} has been replaced by a dot-product involving the $\hat{m}$ values $\{c^{-2}_{K,s}\}_{s=1}^{\hat{m}}$. As a result, the computational cost is multiplied by $\hat{m}$ to construct the matrix.

We emphasize that only the matrix construction computational cost increases. Indeed, the finite element space V_h is unchanged by the MMAm. As a result, the MMAm matrix M has the same size and filling than the one of the standard finite element method, only the values of the coefficients change. Numerical examples will confirm that the inversion of the linear system M is much more costly than the matrix construction. Thus, the overhead of the MMAm is negligible.

We close this section with more details on hypothesis (9) regarding the velocity parameter. Assume that the medium of propagation is highly heterogeneous and that we use the standard finite element method on a non-fitting mesh: the actual velocity parameter is not constant over the cells $K \in \mathcal{T}_h$. In this situation, it is required to define an approximation c_h of c which is constant on each cell $K \in \mathcal{T}_h$ (for instance, by taking $c_h|_K = c_K = c(x_K)$, where x_K is the barycenter of K).

As a result, the standard finite element method requires to approximate c by c_h, where h is the mesh step. In contrast, the MMAm is able to handle an approximation c_ϵ of the velocity parameter c, where the approximation characteristic size $\epsilon \ll h$ can be chosen freely. This is illustrated in Figures 2 and 3.

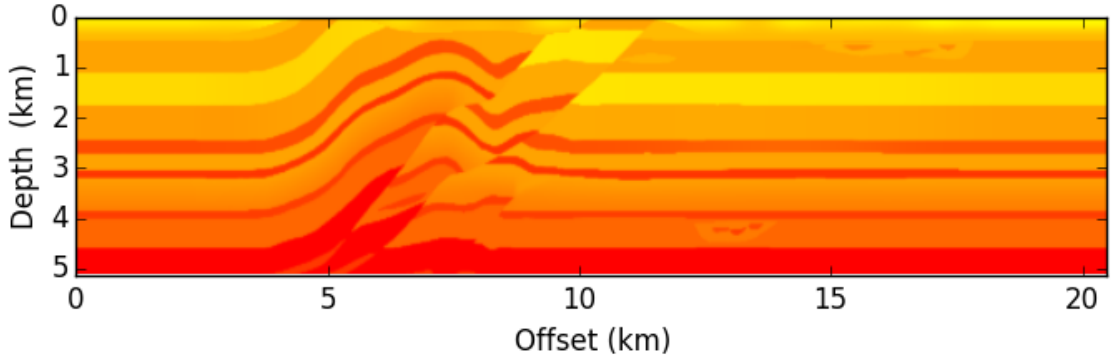

(A) Overthrust P-velocity model

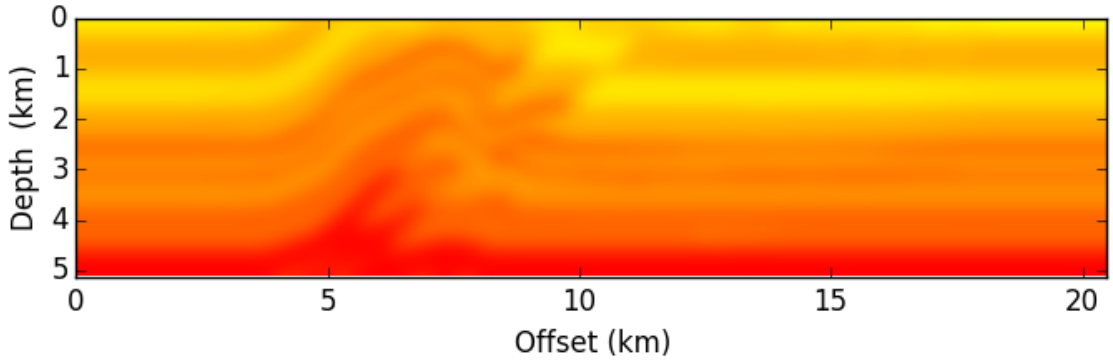

(B) Smoothed overthrust P-velocity model

From the implementation point of view, the MMAm simply amounts to add one loop to the finite element code over the subcells, when assembling the linear system. Since by construction, the integration stencil is the same on all cells, this loop is easily implemented.

As a result, the MMAm turns out to be simpler to implement than existing method in the literature. Actually, the implementation difficulties are comparable to those of a standard FEm.

3. 2D experiments

We consider a slice of the 3D SEG/EAGE overthrust model [4]. The domain of propagation is 20.48 km large and 5.12 km deep. The velocity model is represented by a 512×128 cartesian grid depicted on Figure 4a. The size of each square in the grid defining the characteristic length of the heterogeneities is thus $\eta = 40$ m.

This velocity model features strong contrasts and provides a good benchmark to test the MMAm. However, though the velocity model can be considered as a good idealization of the Earth subsurface, wave propagation is rarely simulated in such a model in actual applications. Indeed, the "true" velocity model is usually unknown and is sought in an inverse procedure, which involves several approximations of the true model which are iteratively improved. Thus, numerical wave propagation takes place in approximate models, which are usually simpler than the true model.

For this reason, we also consider a smoothed version of the model, where a 200 m low-pass filter has been applied to the velocity model. The smoothed version of the velocity model is represented on Figure 4b.

PMLs of length $L = 640$ m are placed on left, right and bottom of the propagation domain. We choose the coefficient $\sigma = 20$.

We consider 100 point-source right-hand-sides located at $z = 50$ m depth. The offsets of the right-hand-sides are equally spaced between 550 and 23530 m. Hence, each right-hand-side

$g = \delta_{(x,z)}$ reads

$$\langle g, v \rangle = \overline{v(x,z)}, \quad \forall v \in \mathcal{D}(\Omega),$$

for a given offset $x \in (550 \text{ m}, 23530 \text{ m})$ and $z = 50$ m.

We compute the wavefields generated by these sources for two different frequencies $f = 5$ and 10 Hz.

Since there is no analytical solution for the problem we consider, we use a reference solution computed on a fine mesh to evaluate the precision of MMAm solutions. The reference solution is computed with standard Lagrangian elements of degree 6. The mesh is based on a cartesian 544×144 grid ($h = 40$ m), each square of the grid being subdivided into two triangles.

Furthermore, to compare finite element solutions computed on different meshes, we evaluate all numerical solutions on a fixed 1024×256 grid. This grid is taken in the computational domain, without the PMLs. Considering a fixed frequency f, for the right-hand-side number $n \in \{1, \dots, 100\}$, we denote by $\bar{u}_{ij}^n$ the value of the reference solution at the node (i, j) of the evaluation grid. Similarly, if u^n is the discrete solution computed on a coarser mesh, we write u_{ij}^n the value of u^n at the node (i, j). Then, we evaluate the accuracy of the method with the error

$$E = \left(\frac{\sum_{n=1}^{100} \sum_{i=1}^{1024} \sum_{j=1}^{256} |\bar{u}_{ij}^n - u_{ij}^n|^2}{\sum_{n=1}^{100} \sum_{i=1}^{1024} \sum_{j=1}^{256} |\bar{u}_{ij}^n|^2} \right)^{1/2}. \tag{12}$$

As the implementation complexity of the MMAm is comparable to that of the standard FEm, it makes sense to give a comparison between the MMAm and the standard FEm.

We employ a FEm which is able to handle constant velocities over each element. We thus approximate the actual velocity by a set of constants defined by

$$c_K = \left(\int_K c^{-2} \right)^{-2}, \tag{13}$$

over K. Averaging formula (13) is motivated by standard periodic homogenization techniques.

We aim at benchmarking different numerical schemes. To distinguish between them, we will focus on the number of degrees of freedom (denoted by "ndf" and corresponding to the dimension of the finite element space) and the number of non-zero elements in the upper triangle of the finite element linear system (denoted by nz; nz is a relevant quantity since we have a symmetric linear system).

We also recall that in the following, h denotes the mesh size, p the polynomial degree and $\hat{m}$ the number of subcells used in the integration scheme. Finally, we will use the letter η to denote the characteristic length the heterogeneities.

3.1. **Original model.** As described above, the method is applied in the original model using different mesh steps, polynomial degrees and frequencies. The percentages of relative error are presented in Tables 1 and 2 for the frequencies $f = 5$ and 10 Hz respectively.

We first observe that if the standard FEm is used together with averaging formula (13), the mesh size h is strongly limited by the characteristic length of the heterogeneities η. Indeed, as shown by the second line of Table 2, taking $h = 2\eta$ at the frequency $f = 10$ Hz does not deliver an accurate solution: the relative error is more than 10%, even if $p = 6$.

On the other hand, it is possible to obtain accurate solutions with less than 1% relative error on coarser meshes with the MMAm. As shown by the third line of Tables 1 and 2, we obtain accurate solutions with $h = 4\eta$ if high order polynomials are used.

This observation explains very well that, even if the medium is strongly heterogeneous, it is possible to let the velocity parameter vary inside the mesh cells with the MMAm.

In order to be more specific about computational cost and to benchmark more precisely the MMAm and the standard FEm, we indicate the number of degrees of freedom (ndf), and the number of non-zero elements in the linear system (nz), required to obtain about 5% accuracy in Table 3. As shown there, it is clear that the MMAm makes it possible to reduce both ndf and nz by 2 for the same accuracy compared to the FEm.

$f = 5$ Hz						
method	error	h	p	$\hat{m}$	ndf	nz
MMAm	5.59%	8η	4	32	0.020	0.241
FEm	6.08%	2η	2	1	0.079	0.491
$f = 10$ Hz						
method	error	h	p	$\hat{m}$	ndf	nz
MMAm	2.42%	2η	3	10	0.177	1.589
FEm	4.96%	η	2	1	0.315	1.962

TABLE 3. Comparison of FEm and MMAm in the original 2D model

3.2. **Smoothed model.** As in the original model, computations are carried out with different choices of h, p and f and the percentages of relative error are presented in Tables 4 and 5 for the frequencies $f = 5$ and 10 Hz respectively.

In the smoothed model, the MMAm performs in the same way than in the original model. It shows that most of the error in MMAm computations is due to numerical dispersion and that the strong contrasts in the velocity model are properly handled.

On the other hand, we see that the standard FEm performs much better in the smoothed model than in the original model. This is because since the model is smooth, less error is generated when averaging the parameter.

Yet, these numerical experiments strongly indicate that the MMAm improves the accuracy of the method, and enables the user to select larger mesh steps.

We propose a comparison between the two methods in Table 6. We see that the MMAm reduces the required number of degrees of freedom by a factor 2. The number of non-zero elements is also reduced.

$f = 5$ Hz						
method	error	h	p	$\hat{m}$	ndf	nz
MMAm	4.00%	8η	4	32	0.020	0.241
FEm	3.29%	4η	3	1	0.045	0.398
$f = 10$ Hz						
method	error	h	p	$\hat{m}$	ndf	nz
MMAm	4.69%	4η	4	10	0.079	0.962
FEm	1.70%	2η	3	1	0.177	1.589

TABLE 6. Comparison of FEm and MMAm in the smoothed 2D model

4. 3D EXPERIMENTS

In order to benchmark the method for 3D applications, we consider a small velocity model featuring a salt body. The domain of propagation is 1280 m $\times$ 1280 m large and 640 m deep. The velocity values are sampled on a $64 \times 64 \times 32$ cartesian grid. It corresponds to a sampling step $\eta = 20$ m. The wavespeed ranges from 1000 ms^{-1} to 5000 ms^{-1}. The velocity model is depicted on Figures 5a, 5b and 5c.

The sides and bottom of the domain are surrounded by PMLs of length $L = 160$ m with coefficient $\sigma = 40$.

We consider a single Gaussian right-hand-side

$$g(x) = \exp\left(-\frac{|x - \overline{x}|^2}{\overline{\sigma}^2}\right),$$

where $\overline{x} = (500, 500, 50)$ m and $\overline{\sigma} = 50$ m.

Cartesian grid based meshes are used in the simulation, each cube of the grid being subdivided into 6 tetrahedron. The reference solution $\bar{u}$ is computed with standard Lagrangian elements of degree 4 with a mesh based on a $80 \times 80 \times 40$ cartesian grid ($h = 20$ m).

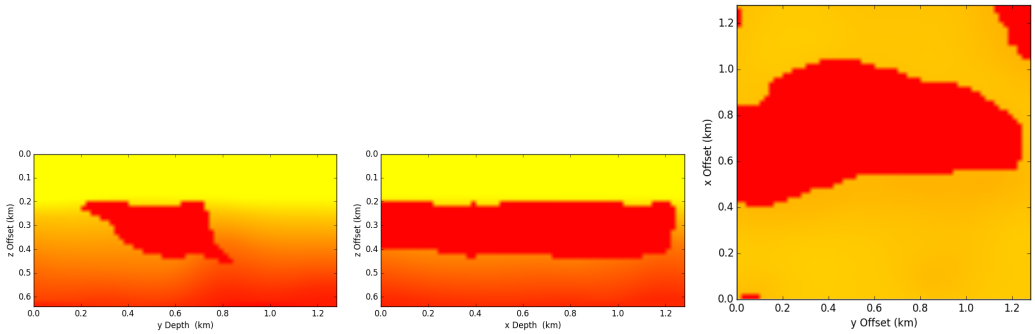

(A) $x = 600$ m cut (B) $y = 600$ m cut (C) $z = 300$ m cut

Numerical solutions are computed on a fixed $128 \times 128 \times 64$ cartesian grid, and the L^2 error of a given numerical solution u is computed with

$$E = \left(\frac{\sum_{i=1}^{128} \sum_{j=1}^{128} \sum_{k=1}^{128} |\bar{u}_{ijk} - u_{ijk}|^2}{\sum_{i=1}^{128} \sum_{j=1}^{128} \sum_{k=1}^{128} |\bar{u}_{ijk}|^2} \right)^{1/2}, \tag{14}$$

where $\bar{u}_{ijk}$ and u_{ijk} are the evaluations of solutions at the node (i, j, k).

In order to benchmark the MMAm with the FEm, we also consider standard Lagrangian discretizations where the velocity parameter is averaged following (13).

It is worth noting that because we use tetrahedron based meshes, it is not easy to exactly fit the cartesian velocity model with a subdivision of the reference tetrahedra. For this reason, we generate a mesh of the reference tetrahedra using the meshing software tetgen. This mesh does not fit the heterogeneities, but we use a sufficiently refined mesh to compute the integrals accurately. We use $\hat{m} = 569$ subcells.

The percentages of relative error are presented in Tables 7 and 8 for the frequencies $f = 5$ and 10 Hz respectively.

Like in the 2D cases, we see that the MMAm is more accurate than the standard FEm and enables the user to select large mesh steps. In particular, if the mesh does not fit the heterogeneities ($h > \eta$), we see that the standard FEm solution using an averaged velocity parameter is less than 5% accurate. On the other hand, MMAm solutions are accurate, even on coarse meshes, if high order polynomials are used.

We compare the MMAm and the standard FEm in Table 9. In particular, we provide computational time which includes the time required for matrix construction, and inversion of the linear system with MUMPS. It is clear that the MMAm speeds up the computations for an equivalent level of accuracy, and the time for matrix construction is negligible as compared to the time for linear system inversion.

$f = 5$ Hz					
method	error	h	p	$\hat{m}$	Time (s)
MMAm	3.88%	8η	4	569	1.1
FEm	2.55%	2η	2	1	16.3
$f = 10$ Hz					
method	error	h	p	$\hat{m}$	Time (s)
MMAm	2.42%	4η	4	569	27.5
FEm	2.80%	η	2	1	315.2

TABLE 9. Comparison of FEm and MMAm in the 3D model

	MMAm						FEm					
h	p=1	p=2	p=3	p=4	p=5	p=6	p=1	p=2	p=3	p=4	p=5	p=6
η (40 m)	58.9	0.497	0.321	0.219	0.162	0	58.9	0.497	0.321	0.219	0.162	0
2η (80 m)	118	3.62	0.682	0.458	0.421	0.418	118	6.08	4.40	4.37	4.37	4.37
4η (160 m)	117	40.9	2.42	1.45	0.998	0.743	116	43.9	16.1	15.9	15.8	15.8
8η (320 m)	108	118	45.8	5.59	2.40	1.93	108	112	64.3	56.1	56.3	56.3

TABLE 1. Original 2D model, $f = 5$ Hz

	MMAm						FEm					
h	p=1	p=2	p=3	p=4	p=5	p=6	p=1	p=2	p=3	p=4	p=5	p=6
η (40m)	127	6.39	0.253	0.171	0.126	0	127	6.39	0.253	0.171	0.126	0
2η (80m)	120	73.6	2.42	0.391	0.332	0.327	120	72.9	17.8	17.6	17.6	17.6
4η (160m)	118	119	77.4	7.59	1.06	0.632	108	117	81.0	52.6	52.6	52.6
8η (320m)	100	107	124	128	75.9	18.5	100	107	121	122	91.3	87.5

TABLE 2. Original 2D model, $f = 10$ Hz

	MMAm						FEm					
h	p=1	p=2	p=3	p=4	p=5	p=6	p=1	p=2	p=3	p=4	p=5	p=6
η (40m)	46.3	0.494	0.336	0.228	0.169	0	46.3	0.494	0.336	0.228	0.169	0
2η (80m)	109	2.73	0.712	0.478	0.440	0.436	109	2.63	0.864	0.702	0.681	0.679
4η (160m)	117	30.3	2.21	1.51	1.04	0.775	117	29.5	3.29	3.06	2.88	2.80
8η (320m)	108	109	31.8	4.00	2.44	2.01	108	109	33.9	22.5	23.4	23.3

TABLE 4. Smoothed 2D model, $f = 5$ Hz

	MMAm						FEm					
h	p=1	p=2	p=3	p=4	p=5	p=6	p=1	p=2	p=3	p=4	p=5	p=6
η (40m)	119	4.69	0.268	0.181	0.134	0	119	4.69	0.268	0.181	0.134	0
2η (80m)	123	56.5	1.65	0.392	0.352	0.347	123	56.2	1.70	1.12	1.12	1.11
4η (160m)	108	112	56.9	4.69	0.939	0.650	108	112	55.4	13.3	13.5	13.6
8η (320m)	100	108	123	115	50.4	9.73	100	109	123	115	51.4	33.5

TABLE 5. Smoothed 2D model, $f = 10$ Hz

	MMAm						FEm					
h	p=1	p=2	p=3	p=4	p=5	p=6	p=1	p=2	p=3	p=4	p=5	p=6
η (20m)	10.4	0.370	0.410	0	x	x	10.4	0.370	0.410	0	x	x
2η (40m)	35.8	2.02	1.93	1.92	1.91	x	36.5	2.55	2.33	2.35	2.42	x
4η (80m)	88.6	9.12	3.57	3.52	3.54	3.53	89.9	13.9	8.81	8.72	8.75	8.86
8η (160m)	126	55.5	10.9	3.88	3.67	3.66	127	62.6	2020	21.1	20.9	21.0

TABLE 7. 3D model, $f = 5$ Hz

	MMAm						FEm					
h	p=1	p=2	p=3	p=4	p=5	p=6	p=1	p=2	p=3	p=4	p=5	p=6
η (20m)	66.0	2.80	2.50	0	x	x	66.0	2.80	2.50	0	x	x
2η (40m)	113	15.3	3.40	3.77	3.53	x	114	21.4	15.3	11.7	11.5	x
4η (80m)	135	84.8	17.1	4.89	4.62	4.65	131	91.1	37.8	30.9	30.6	30.8
8η (160m)	108	123	93.9	51.6	17.4	6.53	107	128	101	77.3	68.2	61.7

TABLE 8. 3D model, $f = 10$ Hz

5. Conclusion

In this work, we have proposed a straightforward method for heterogeneous Helmholtz problems: the Multiscale Medium Approximation method (MMAm). For the sake of simplicity, we have focused on the case of acoustic problems with constant density. The MMAm can be viewed as a special integration technique, which makes it possible to incorporate small scale informations at a low computational price. The precise formula that need to be implemented are stated.

We have tested the MMAm on 2D and 3D geophysical benchmarks. In 2D, we have considered the Overthrust velocity model. In order to represent actual applications that happen within an inverse procedure, we have considered both the original model and a smooth version. The 3D model represented a salt body.

As the MMAm turns out to be as simple to implement as a standard FEm, it makes sense to benchmark it against standard elements. We carry out this comparison by using standard finite elements with an upscaled velocity parameter computed thanks to an averaging formula.

The comparison includes a discussion on the size and filling of the linear systems for 2D benchmarks, and a discussion on computational times for the 3D benchmark. For the considered frequencies (5 and 10 Hz), our examples show that the MMAm enables the user to select mesh steps much larger than the characteristic length of the heterogeneities. As a result, the number of degrees of freedom required for an equivalent precision can be reduced up to a factor 4. Concerning computational times, the MMAm speeds up our 3D benchmark by more than a factor 10.

We conclude that in the simple setting of acoustic wave propagation with constant density, the MMAm permits to significantly increase the computational efficiency of forward modeling in the frequency range commonly used in Full Waveform Inversion (up to 10 Hz). It is worth noting that though we focus on implementation and testing in this paper, a theoretical convergence analysis is available [8, 14], which is in accordance with the present results.

Future works include the application of the MMAm to non-constant density acoustic wave propagation and elastic wave propagation as well as time dependent problems.

6. Acknowledgements

This work was partially supported by the project M2NUM (M2NUM is co-financed by the European Union with the European regional development fund (ERDF, HN0002137) and by the Normandie Regional Council.") and the INRIA-TOTAL strategic action DIP (`http://dip.inria.fr`).

H. Barucq and Théophile Chaumont-Frelet have received funding from the European Union's Horizon 2020 research and innovation programme under the Marie Sklodowska-Curie grant agreement No 644602.

Théophile Chaumont-Frelet has received funding from the Projects of the Spanish Ministry of Economy and Competitiveness with reference MTM2016-76329-R, and the BCAM "Severo Ochoa" accreditation of excellence SEV-2013-0323.

The authors also thank the Centre for Computer Resources of Normandy (CRIANN, `http://www.criann.fr`) where numerical simulations have been carried out.

References

[1] M. Ainsworth, *Discrete dipersion relation for hp-version finite element approximation at high wave number*, SIAM J. Numer. Anal. **42** (2004), no. 2, 553–575.

[2] G. Allaire, *Homogenization and two-scale convergence*, SIAM J. Math. Anal. **23** (1992), no. 6, 1482–1518.

[3] P. Amestoy, R. Brossier, J.Y. L'Excellent, T. Mary, L. Métivier, A. Miniussi, and S. Operto, *Fast 3d frequency-doamin full waveform inversion with a parallel block low-rank multifrontal direct solver: application to obc data from the north sea*, Geophysics, in press (2016).

[4] F. Aminzadeh, B. Jean, N. Burkhard, J. Long, T. Kunz, and P. Duclos, *Three dimensional seg/eaeg models – an update*, The Leading Edge **15** (1996), no. 2, 131–134.

[5] I. Babuska, F. Ihlenburg, E. T. Paik, and S.A. Sauter, *A generalized finite element method for solving the helmholtz equation in to dimensions with minimal pollution*, Comput. Methods Appl. Engrg. **128** (1995), 325–359.

[6] G.E. Backus, *Long-wave anisotropy produced by horizontal layering*, J. Geophys. Res. **67** (1962), 4427–4440.

[7] C. Baldassari, H. Barucq, H. Calandra, B. Denel, and J. Diaz, *Perfomance analysis of a high-order discontinuous galerkin method. application to the reverse time migration*, Communcations in Computational Physics **11** (2012), no. 2, 660–673.
[8] H. Barucq, T. Chaumont-Frelet, and C. Gout, *Stability analysis of heterogeneous helmholtz problems and finite element solution based on propagation media approximation*, Math. of Comp. **86** (2017), no. 103, 2129–2157.
[9] Y. Capdeville, L. Guillot, and J.-J. Marigo, *1-d non-periodic homogenization for the seismisc wave equation*, Geophys. J. Int. **181** (2010), 897–910.
[10] ———, *2-d non-periodic homogenization of the elastic wave equation: Sh wave*, Geophys. J. Int. **182** (2010), 1438–1454.
[11] ———, *2-d non-periodic homogenization to upscale elastic media for p-sv waves*, Geophys. J. Int. **182** (2010), 903–922.
[12] Y. Capdeville and J.-J. Marigo, *Second order homogenization of the elastic wave equation for non-periodic layered media*, Geophys. J. Int. **170** (2007), 823–838.
[13] J.M. Carcione, D. Kosloff, and A. Behle, *Long-wave anisotropy in stratified media: A numerical test*, Geophysics **56** (1991), no. 2, 245–254.
[14] T. Chaumont-Frelet, *Finite element approximation of helmholtz problems with application to seismic wave propagation*, PhD Thesis, https://tel.archives-ouvertes.fr/tel-01246244 (2015).
[15] ———, *On high order methods for the heterogeneous helmholtz equation*, CAMWA **72** (2016), 2203–2225.
[16] D. Cioranescu, A. Damlamian, and G. Griso, *The periodic unfolding method in homogenization*, SIAM J. Math. Anal. **40** (2008), no. 4, 1585–1620.
[17] F. Ihlenburg and I. Babuška, *Finite element solution of the helmholtz equation with high wave number part ii: the h-p version of the fem*, SIAM J. Numer. Anal. **34** (1997), no. 1, 315–358.
[18] D. Komatitsch and J. Tromp, *A perfectly matched layer absorbing boundary condition for the second-order seismic wave equation*, Geophys. J. Int. **154** (2003), 146–153.
[19] V. Lisitsa, G. Reshetova, and V. Tcheverda, *Finite-difference algorithm with local time-space grid refinement for simulation of waves*, Comput Geosci **16** (2012), 39–54.
[20] J.M. Melenk and S. Sauter, *Wavenumber explicit convergence analysis for galerkin discretizations of the helmholtz equation*, SIAM J. NUMER. ANAL. **49** (2011), no. 3, 1210–1243.
[21] L. Sirgue and R.G. Pratt, *Efficient waveform inversion and imaging: A strategy for selecting temporal frequencies*, Geophysics **69** (2003), no. 1, 231–248.